



Predicting clinical physiology: A Markov chain model of heart rate recovery after spontaneous breathing trials in mechanically ventilated patients[☆]

Yan Lu PhD^{a,1}, Anton Burykin PhD^{b,1},
Michael W. Deem PhD^a, Timothy G. Buchman PhD, MD^{b,*}

^aDepartment of Physics and Astronomy, Rice University, Houston, TX 77005, USA

^bDepartment of Surgery, Washington University, Saint Louis, MO 63110, USA

Keywords:

Heart rate variability;
Heart rate recovery;
Mechanical ventilation;
Spontaneous breathing trial;
Physiologic stress;
Markov chain;
Fluctuation-dissipation theorem;
Poincaré plot

Abstract Analysis of heart rate (HR) dynamics before, during, and after a physiologic stress has clinical importance. For example, the celerity of heart rate recovery (HRR) after a cardiac stress test (eg, treadmill exercise test) has been shown to be an independent predictor of all-cause mortality. Heart rate dynamics are modulated, in part, by the autonomic nervous system. These dynamics are commonly abstracted using metrics of heart rate variability (HRV), which are known to be sensitive to the influence of the autonomic nervous system on HR. The patient-specific modulators of HR should be reflected both in the response to stress as well as in the recovery from stress. We therefore hypothesized that the patient-specific HR response to stress could be used to predict the HRR after the stress.

We devised a Markov chain model to predict the poststress HRR dynamics using the parameters (transition matrix) calculated from HR data during the stress. The model correctly predicts the exponential shape of poststress HRR. This model features a simple analytical relationship linking poststress HRR time constant (T_{off}) with a standard measure of HRV, namely the correlation coefficient of the Poincaré plot (first return map) of the HR recorded during the stress. A corresponding relationship exists between the time constant (T_{on}) of R-R interval decrease at the onset of stress and the correlation coefficient of the Poincaré plot of prestress R-R intervals. Consequently, the model can be used for the prediction of poststress HRR using the HRV measured during the stress. This direct relationship between the event-to-event *microscopic fluctuations* (HRV) during the stress and the *macroscopic response* (HRR) after the stress terminates can be interpreted as an instance of a fluctuation-dissipation relationship. We have thus applied the fluctuation-dissipation theorem to the analysis of heart rate dynamics.

The approach is specific neither to cardiac physiology nor to transitions between mechanical and free ventilation as a specific stress. It may therefore have wider applicability to physiologic systems subject to modest stresses.

© 2009 Elsevier Inc. All rights reserved.

[☆] This work was generously supported by grants from the James S. McDonnell Foundation (220020070), DARPA (49533-LS-DRP and HR0011-05-1-0057), and the Barnes-Jewish Hospital Foundation.

* Corresponding author.

E-mail address: buchman@wustl.edu (T.G. Buchman).

¹ These authors contributed equally to the work.

1. Introduction and overview

During a physiologic stress, the heart rate (frequency of the heart)² is modulated by both sympathetic and parasympathetic (vagal) branches of autonomic nervous system (ANS) [1]. Using the familiar example of intense exercise, the HR increases due to parasympathetic inhibition and sympathetic activation. Reciprocally, during cooldown after exercise, the HR decreases because of parasympathetic activation and sympathetic inhibition [2]. It is believed that parasympathetic effect is dominant [1,3-6]. The celerity of heart rate recovery (HRR) after a stress has significant clinical importance as a diagnostic and prognostic index [7-11]. Imai et al [3] first demonstrated that HRR was faster in well trained athletes but prolonged in patients with chronic heart failure. HRR has been shown to be an independent predictor of mortality [8,9,12-14].

HRR kinetics (“off-response”) are conveniently quantified with a time constant (T_{off}) obtained from the first order exponential fit of HR data (see, however, Ref. [14]). A corresponding time constant T_{on} obtained from the first order exponential fit of HR acceleration characterizes the “on-response” of HR to the stress. Compared to the recovery kinetics, HR acceleration kinetics at the onset of the stress has been studied less intensively [15-18].

Because the ANS modulates both the HR relaxation dynamics during the HRR as well as HR fluctuations (“variability”) under steady-state (“equilibrium”) conditions, many studies (see, eg, Refs. [4,15,19]) have focused on the assessment of HRR using different (especially vagal-related) indices of heart rate variability (HRV)³ [20]. Given that both reduced HRV as well as prolonged HRR are believed to be predictors of mortality (or at least markers of reduced vagal activity), a common hypothesis [15] is that the HRR time is inversely proportional to some index or measure of HRV,

$$T_{off}(HRR) \sim \frac{1}{HRV\ index} \quad (1)$$

To test that hypothesis, most of the prior studies (see, however, Ref. [23]) have employed conventional statistical

tools (parametric or nonparametric correlation coefficients) to explore empirical correlations between HRR time constants and different measures of HRV during (or after) the exercise.

Herein, we adopt an alternative strategy, deriving the relationship Eq. (1) theoretically rather than empirically (statistically) inferring it from the data. We apply the fluctuation-dissipation theorem, which relates the system response to a relatively small perturbation to the fluctuations in the stationary state of the system [24,25].

More specifically, we characterize a deliberate clinical stress as a uniform perturbation of HR dynamics that changes the HR to a new steady state. When the stress is relieved, the HR dynamics relax towards the prestress state. The stress is modest, justifying the use of a linear-response formalism to predict the HR relaxation. We can then model the relaxation dynamics by a Markov chain [26] with Gaussian probability distributions calculated from the HR data during the stress⁴.

We test the model predictions with data recorded during spontaneous breathing trials (SBTs) of mechanically ventilated critically ill patients in an intensive care unit (ICU). Spontaneous breathing trials constitute well-defined but modest physiologic stresses (see, eg, Ref. [27] and references therein) that are (serially) used in the ICU to determine patients’ readiness for liberation from the mechanical ventilator. Spontaneous breathing through a long and somewhat narrow tube without mechanical assistance requires incremental effort over nose and mouth breathing (Poiseuille law). Not all patients complete the full SBT, a clinical situation analogous to the early termination of a cardiac treadmill stress test in ambulatory patients.

The balance of this report is organized as follows. In the next section, we review the SBT procedure; compare it to a treadmill stress test; and describe patient selection, HR data recording and preprocessing. In Section 3, we present the derivation of the Markov chain model and discuss how the model predictions are related to the standard HRR and HRV measures. Then, in Section 4, we show the result of the test of our model for the prediction of HRR in ICU patients after the SBT. Finally, in Section 5, we consider the limitation of both our clinical SBT data sets and the developed model and highlight possible improvements and generalizations of the proposed approach. We also discuss other physiological signals and clinical procedures (both in the ICU and elsewhere) that can be analyzed using the

² In this report, the terms “(instantaneous) heart rate” and “frequency of the heart” are taken to be synonymous. The first term, measured in beats per minute, is common in physiology and medicine. The second term, measured in hertz, is common in (bio)physics. The two differ only by a factor. For consistency in the article, units of hertz are used throughout.

³ The term “heart rate variability” [20] is used to describe variations of the time intervals T_{RR} (usually measured in milliseconds) between consecutive heart beats (so-called R-R intervals) not the instantaneous heart rate f_{heart} itself ($f_{heart} = 1/T_{RR}$). Thus, one should distinguish between the measures of R-R interval variability (HRV) and HR variability (even though there are one-to-one relationships between them). Throughout the article (unless otherwise specified), we study only the fluctuations of the instantaneous heart rate, not R-R intervals. More about the differences between HR and R-R variability measures can be found, for example, in Refs. [21,22].

⁴ A Markov chain is defined as a stochastic process with the Markov property. The Markov property means that the probability of the future states depend only on the present state and is independent of any prior states [26]. Herein, it means that the instantaneous heart rate associated with the current beat fully captures all information that could possibly influence subsequent heartbeats. Thus, future instantaneous heart rates arise through a probabilistic—not deterministic—process.

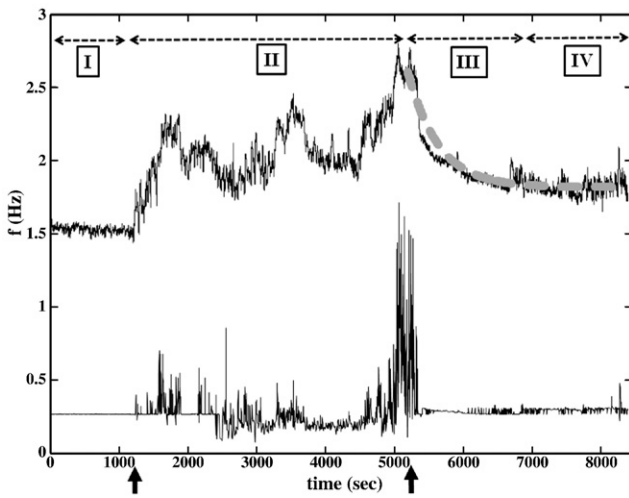


Fig. 1 Heart rate of patient P05 during the 2 h 30 m time interval (before, during and after the SBT) (top, solid line). Markov chain model prediction of the heart rate relaxation in phase III (top, dashed line); Respiration rate of the patient P05 during the same time interval (bottom, solid line). Arrows on the time axis (at the bottom) indicate the beginning and the end of SBT. We divide the whole duration of the data set into four time intervals, or “phases” (indicated on the figure as I, II, III and IV, respectively, see text for details).

proposed model. Based on the observations, we infer a possible clinical importance of HRR dynamics after SBT. The clinical relevance of HRR has not previously been assessed even if the HRV changes during the weaning from mechanical ventilator have been studied (see, eg, Ref. [28]).

2. Spontaneous breathing trial as a stressor

2.1. Spontaneous breathing trial procedure; comparison to an exercise stress test

The SBT is standard clinical practice used to evaluate the readiness of patients for liberation from mechanical ventilatory support. The detailed description of the SBT procedure used in this study is given elsewhere [29]. The SBT is planned to be 30-minute period of spontaneous ventilation bracketed by similar intervals of mechanical ventilatory support. The total time (~90 minutes) can be recast into four subintervals or “phases” (Fig. 1). We designate the subinterval from the beginning of each data set to the beginning of the SBT as “phase I” (during this subinterval, gas exchange is driven by a mechanical ventilator and the heart rate is relatively stationary). The SBT time interval is “phase II” (this time interval corresponds to spontaneous ventilation, and the heart rate is typically significantly higher in phase II than in phase I owing to the sympathetic response to the stress). The subinterval after the end of SBT when the heart rate is relaxing to a new steady state value is “phase III.” Finally, the subinterval from the moment when the heart rate becomes stationary again to the end of the data set is “phase IV.” Comparing an SBT to a typical ambulatory treadmill stress test, phase I corresponds to the pre-exercise part of the stress test, phase II (which is stress) corresponds to the exercise itself, and phases III and IV correspond to the postexercise part. HRR occurs as phase III.

Table 1 Demographics, sedation score and sedating medications at the time of the breathing trial

Patient	Data set	Ethnicity	Sex	Age	Modified Ramsay score (sedation level)	Analgesics and anxiolytics
P01	D01	Caucasian	Male	36	4	None
P02	D02	Caucasian	Male	61	3	Fentanyl, midazolam
P03	D03	Caucasian	Male	52	3	Fentanyl
P04	D04	Caucasian	Female	45	2	Fentanyl
P05	D05	African-American	Female	17	2	Fentanyl
P06	D06	Caucasian	Male	69	4	Fentanyl, midazolam
P07	D07	Caucasian	Female	71	4	Fentanyl, propofol
P08	D08	African-American	Male	22	4	Fentanyl, midazolam
	D09	African-American	Male	22	3	Fentanyl, midazolam
	D10	African-American	Male	22	1	Fentanyl, midazolam
P09	D11	Caucasian	Female	52	2	None
P10	D12	African-American	Female	34	2	Fentanyl, midazolam
P11	D13	African-American	Female	69	4	Fentanyl, midazolam
P12	D14	Caucasian	Female	32	4	Fentanyl, propofol
	D15	Caucasian	Female	32	4	Fentanyl
P13	D16	Caucasian	Male	27	3	Fentanyl
	D17	Caucasian	Male	27	2	Fentanyl, propofol
P14	D18	Caucasian	Male	61	2	Fentanyl, midazolam
P15	D19	African-American	Female	80	1	Fentanyl, propofol
P16	D20	Caucasian	Female	37	1	Fentanyl

2.2. Patient selection; clinical conditions

Because the purpose of this preliminary study is to investigate the heart rate relaxation after the end of SBT, we used a convenience sample of 16 patients (coded alphanumerically from P01 to P16), chosen because their physiological signals were mostly free of artifacts, who tolerated a 30-minute SBT without adverse physiologic consequence, and whose heart rate significantly changed during the SBT. Coincidentally, we collected 3 data sets for the patient P08 and 2 data sets for each of the patients P12 and P13. These data sets correspond to the different SBTs performed at different days. Thus, the total number of data sets analyzed was 20 (they were coded alphanumerically from D01 to D20).

Sedating drugs routinely prescribed to relieve patient anxiety were diminished or discontinued prior to the data collection. Demographic data, sedation level (modified Ramsay score), and sedating drugs prescribed to all 16 patients are collected in Table 1. This pilot study group consists of 7 men and 9 women with age range from 17 to

80 years (47.9 ± 19.2 years). This observational study was approved by the Washington University Human Research Protections Organization.

2.3. Data collection and preprocessing

A detailed description of the data collection and analysis procedure can be found elsewhere [30]. Briefly, we used Philips IntelliVue M70 bedside monitors and Ixellence TrendFace software (<http://www.ixellence.com>) to continuously collect electrocardiogram (at 500 Hz sampling frequency) and end-tidal CO₂ (capnography) waveform (at 62.5 Hz sampling rate) as a respiratory signal. KubiosHRV software (Biosignal Analysis and Medical Imaging Group, Department of Physics, University of Kuopio, Finland) [31] was used to extract heart rate intervals (R-R intervals) from single-lead 500 Hz electrocardiogram signals. Heart and respiration rates (frequencies) were computed as the inverse of the beat-to-beat (R-R) and breath-to-breath intervals, for example, $f_{\text{heart}}(k) = 1/T_{\text{RR}}(k)$.

3. Markov chain model

3.1. Formulation of the model

The goal is to predict, using a Markov Chain model, the HR dynamics during the phase III (HRR) from (a) HR dynamics during the phase II (SBT) and (b) the final steady state value in phase IV.⁵

Pertinent to the model are 2 key assumptions about phase II. First, the probability distribution of the heart rate $f(t)$ is a Gaussian. Second, the joint probability distribution of the heart rate at times $t - \Delta t$ and t (where $\Delta t = t_{k+1} - t_k$ is the “sampling time” [time interval between consecutive data points]) is a 2-dimensional Gaussian (see Ref. [32]). These probability distributions are:

$$p[f(t)] = \frac{1}{\sqrt{2\pi\langle\delta f^2\rangle}} \exp\left[-\frac{1}{2} \frac{\delta f(t)^2}{\langle\delta f^2\rangle}\right] \quad (2)$$

$$p(f(t-\Delta t), f(t)) = \frac{1}{2\pi\sqrt{|M|}} \exp\left\{-\frac{1}{2} [\delta f(t-\Delta t), \delta f(t)]^T M^{-1} [\delta f(t-\Delta t), \delta f(t)]\right\}, \quad (3)$$

where $\delta f(t) = f(t) - \langle f \rangle$, $\langle f \rangle$ is the mean HR (everywhere in the article, the brackets $\langle \rangle$ define the average values), superscript ^T signifies transposition, and M is the 2×2 variance-covariance matrix defined as follows:

$$M = \begin{pmatrix} \langle\delta f(t-\Delta t)^2\rangle & \langle\delta f(t)\delta f(t-\Delta t)\rangle \\ \langle\delta f(t-\Delta t)\delta f(t)\rangle & \langle\delta f(t)^2\rangle \end{pmatrix} \equiv \begin{pmatrix} \langle\delta f(t)^2\rangle & \langle\delta f(t-\Delta t)\delta f(t)\rangle \\ \langle\delta f(t-\Delta t)\delta f(t)\rangle & \langle\delta f(t)^2\rangle \end{pmatrix} \quad (4)$$

Here M^{-1} is the inverse of M , and $|M|$ is the determinant of M .

We assume that heart rate dynamics in phase II are stationary in the “wide-sense” (also known as “weak sense” or “covariance stationary” when only the mean and the standard deviation of the process are constant); thus, $\langle\delta f(t-\Delta t)^2\rangle = \langle\delta f(t)^2\rangle$, $\langle\delta f(t-\Delta t)\delta f(t)\rangle = \langle\delta f(t)\delta f(t-\Delta t)\rangle$, and therefore, the variance-covariance and transition matrices do not depend on time. Finally, the conditional probability is defined as:

$$R(f(t)|f(t-\Delta t)) = \frac{p(f(t-\Delta t), f(t))}{p(f(t-\Delta t))} = \sqrt{\frac{\langle\delta f(t)^2\rangle}{2\pi|M|}} \exp\left\{-\frac{1}{2} [\delta f(t-\Delta t), \delta f(t)]^T M^{-1} [\delta f(t-\Delta t), \delta f(t)] + \frac{1}{2} \frac{\delta f(t-\Delta t)^2}{\langle\delta f(t)^2\rangle}\right\} \quad (5)$$

⁵ In this pilot study, the goal was to predict the dynamics of the relaxation curve and not the final value. For this reason, we assumed knowledge of the average final heart rate seen in phase IV, which was frequently different than the average prestress heart rate in phase I. Such hysteresis is commonly observed in ambulatory stress tests. Predictions of the shape of the phase III relaxation based only the phase I prestress heart rate and phase II variability were adequate but less accurate.

After $R(f(t)|f(t - \Delta t))$ is normalized by column, we obtain the one-time-step transition matrix. Using this one-step transition matrix, we can construct the Markov chain so that the probability vector $P(t_k)$ at time t_k is given by

$$P(t_k) = R^k \cdot P(t_0) \quad (6)$$

Finally, the HR at time t_k is an ensemble average over all N states:

$$\langle f(t_k) \rangle = \sum_{n=1}^N f_n \cdot P_n(t_k) = \sum_{j=1}^N \sum_{i=1}^N f_i \cdot [R^k]_{ij} \cdot P_j(t_0) \quad (7)$$

Next, we apply the fluctuation-dissipation theorem to the stress-to-relaxation (phase II-phase III) transition. We consider the interval of spontaneous breathing (phase II) to be a constant perturbation of the HR dynamics (the perturbation has been “on” sufficiently long that transients have died out and the HR has reached a new steady-state [or “equilibrium” state]). The perturbation (the demands of spontaneous breathing through an artificial tube) is then “switched off.” With a modest clinical perturbation, the linear response theory formalism applies and can be used directly to model the HR relaxation (phase III) to the new equilibrium (which is HR at rest, phase IV) by employing the “equilibrium” probability distributions. More specifically, we solve the Markov chain model [Eq. (7)] for heart rate in phase III with the variance-covariance matrix M [Eq. (4)] and one-step transition matrix \mathbf{R} [Eq. (5)] calculated from the phase II data.

In general, Eq. (6) must be solved numerically. However, in the particular case of the assumed Gaussian probability distributions [Eqs. (2-3)], we readily obtain an analytical solution (the complete derivation is given in Appendix C):

$$\langle f(t_k) \rangle_{III} = \langle f \rangle_{IV} + (f_0 - \langle f \rangle_{IV}) \cdot [r_{ff}(\Delta t)]^{\frac{t_k - t_0}{\Delta t}} = \langle f \rangle_{IV} + (f_0 - \langle f \rangle_{IV}) \cdot \exp[-(t_k - t_0)/T_{off}] \quad (8)$$

Here, $f(t_0) = f_0$ is the initial heart rate at the beginning of phase III (we denote this time as t_0), $\langle f \rangle_{IV}$ is the final steady state heart rate and $t_k = t_0 + k\Delta t$, using the same sampling time Δt in the phase II variance covariance matrix as in the relaxation dynamics during the phase III.⁶ We also use the following notations:

$$r_{ff}(\Delta t) = \frac{\langle \delta f(t - \Delta t) \delta f(t) \rangle}{\langle \delta f(t)^2 \rangle} \quad (9)$$

$$T_{off} = \frac{\Delta t}{|\ln[r_{ff}(\Delta t)]|} \quad (10)$$

3.2. Model analysis

Eqs. (8) to (10) prompt several observations. First, pure theory generated the exponential shape of HRR after the stress. Exponentials are the empirical forms most frequently chosen for statistical fit of experimental HRR data. Second, $r_{ff}(\Delta t)$ (Eq. (9)) is a standard HRV index, namely, the correlation coefficient of Poincaré plot [return map $f(t)$ vs. $f(t - \Delta t)$] [33-35] calculated for HR data from the stress (phase II). Because T_{off} is the HRR time constant, Eq. (10) resembles Eq. (1). We thus derive theoretically the relationship between HRV index during the stress [$r_{ff}(\Delta t)$] and the poststress HRR time constant (T_{off}). Finally, note that Eq. (10) is the definition of the relaxation time of the autocorrelation function of the first-order autoregressive process $AR(1)$ [36] (see Appendix B). However, in contrast to the usual definition, r_{ff} and T_{off} in Eq. (10) belong to two processes: r_{ff} is calculated from the *microscopic fluctuations* during the phase II, and T_{off} characterizes the *macroscopic relaxation* during phase III. This connection reflects our assertion that the fluctuation-dissipation theorem is applicable: fluctuations embedded in the variance-covariance matrix obtained during phase II are used to model the HR dynamics during phase III. The direct relation of the Eq. (10) to the AR(1) autocorrelation function and fluctuation-dissipation theorem is elaborated in Appendix A.

Poincaré plots for different values of the sampling time Δt are related to the so-called lagged Poincaré plots [35]^{7,8}.

⁶ The difference $\Delta f = f_0 - \langle f \rangle_{IV}$ that appears in Eq. (8) is often called the HR reserve [14].

⁷ Note that by changing the sampling time Δt , one can obtain a set of relaxation times T_{off} . Such a strategy yields “coarse graining” and provides for multiscale HRR analysis [37] (see also Appendix B).

⁸ Selection of the sampling time Δt requires careful consideration, since it is directly related to the interpretation of Eq. (10). We model HR dynamics as a Markov chain with Gaussian transition probabilities. Thus, the variance-covariance matrix \mathbf{M} fully describes the modeled process. So if any resampling is used, the variance-covariance matrix \mathbf{M} of the resampled dataset should be similar to those of the original, “raw” heart rate data. This is especially important for the covariance term M_{21} , which captures “one-step” fluctuations of the heart rate. The raw HR is an intrinsically discrete, point process (“spike-train”). For the raw HR data (or for relatively large Δt), M_{21} reflects real heart rate fluctuations. However when Δt is very small, M_{21} reflects mostly one-step fluctuations of the interpolated data points, which begins to reflect the variability of the interpolation method rather than the original HR. The parameter Δt must therefore be chosen large enough for the Markov approximation to be valid. The resampling frequency (Δt^{-1}) should not be significantly larger than the maximum HR.

In addition, one can obtain relationship identical to Eq. (10) between the time constant (T_{on}) of R-R interval decrease at the onset of stress (“on response”) and the correlation coefficient of the Poincaré plot of prestress R-R intervals:

$$T_{on} = \frac{\Delta t}{|\ln[r_{RR}(\Delta t)]|} \quad (11)$$

3.3. Numerical solution and simulation

We confirmed our theoretical results [Eq. (10)] by direct numerical solution of Eq. (6) using the HR data recorded during and after the SBT. Below we describe the details of our simulations.

First, we defined the range of heart rate fluctuations. Typically HR varied from 0.5 Hz (30 beats per minute) to 3 Hz (180 beats per minute). We set $f_{\min} = 0.5$ Hz (30 beats per minute) for nearly every patient to account for occasional bradycardia. In order to keep the transition probabilities symmetric, we defined maximum heart rate as $f_{\max} = 2\langle f_j \rangle - f_{\min}$, where $\langle f_j \rangle$ is the mean heart rate for j th data set in phase IV ($j = 1, \dots, 20$). Thus f_{\max} is different for different data sets and varies from 1.5 to 3.5 Hz.

Next, we divided the range $[f_{\min}, f_{\max}]$ of into $N = 400$ equally spaced bins, so each of these bins defines a state S_n in our model⁹:

$$S_n = S_{\min} + nL, \quad (12)$$

Here, $n = 1, \dots, N$, L is the bin size defined as $L = (S_{\max} - S_{\min})/N$, $S_{\min} = f_{\min}$, and $S_{\max} = f_{\max}$. Then, we discretized our time series and interpolated the time series so that if at a moment of time t , the heart rate $f(t)$ is within n th bin, then we put

$$f(t) = S_n - 0.5 \cdot L \quad (13)$$

Thus, the $N \times N$ matrix \mathbf{R} [Eq. (5)] defined the one step conditional probability density for the transition from the current state S_n to the state S_m for the unit time step, Δt , where Δt is the inverse average HR for the data set: $\Delta t = \langle f \rangle^{-1}$.

The initial probability distribution $P(t_0)$ is defined as follows. If the heart rate at the initial moment of time t_0 (at the beginning of the phase III) was in the m th bin, then the n th elements of the $P(t_0)$ vector are defined as follows: $P_n(t_0) = \delta_{n,m}$, $n = 1, N$ (ie, a Kronecker δ symbol such that all vector components are equal to zero, except the m th component, which is equal to 1).

Finally, our prediction of heart rate at the time t_k during phase III is the ensemble average over all states S :

$$\langle f \rangle_S(t_k) = \sum_{n=1}^N (S_n - 0.5 \cdot L) \cdot P_n(t_k) \quad (14)$$

4. Results: prediction of the HRR after SBT

We accurately predicted the heart rate relaxation for 17 of 20 data sets (meaning that we succeeded in predicting nearly all of the data points). For some HRR data sets, we succeeded in predicting most of the data points. However, these data sets had “spikes” (impulses) that we were unable to predict. Finally, some data sets failed to predict most of the points and therefore failed to predict the shape of the decay (see, eg, Fig. 2).

To estimate the accuracy of the model prediction, we calculated (see Table 2) mean absolute percentage error (MAPE):

$$\varepsilon_{dm} = \frac{1}{K} \sum_{k=1}^K \frac{|f_{data}(k) - f_{mod}(k)|}{|f_{data}(k)|} \cdot 100\% \quad (15)$$

Here, f_{data} and f_{mod} are observed and predicted heart rates, respectively, and K is the number of data points. The MAPE error is proportional to the distance (in $L1$ norm) between f_{data} and f_{mod} vectors (data sets).

It is, however, not quite correct to compare the prediction directly to the observed relaxation data since our model can predict only exponential relaxations [in the form of Eq. (8)]. Because the “best exponent” that can describe HRR data sets is the exponential fit of these data sets, the best prediction one can get with our model must be very close (or identical) to the exponential fit. Thus, in order to estimate the prediction error more accurately, we decomposed the total error ε_{dm} into 2 parts: ε_{df} , the distance (MAPE error) between observed HR data sets and their exponential fits, and ε_{mf} , the distance (MAPE error) between predicted HR and exponential fit of observed HR data sets (Table 2). The ε_{mf} gives the actual the accuracy of the prediction, while ε_{df} is a “systematic” error (due to our assumption of the exponential shape of HRR). By optimizing model parameters, one can minimize the ε_{mf} error (the prediction will be very close to the exponential fit), but the ε_{df} error cannot be minimized (some of the HRR have obvious non-exponential shape, see, eg, Fig. 2). So, in the case of nonexponential relaxation, the model simply cannot reproduce it, no matter how accurate the model parameters. In such cases, the ε_{df} error (and as a consequence ε_{dm} error) will necessarily be large. Thus, ε_{df} can be viewed as a measure of nonexponentiality of the HRR.

⁹ Not all bins will be occupied. Among our patients, from 28.5% to 90.5% of the bins were unoccupied.

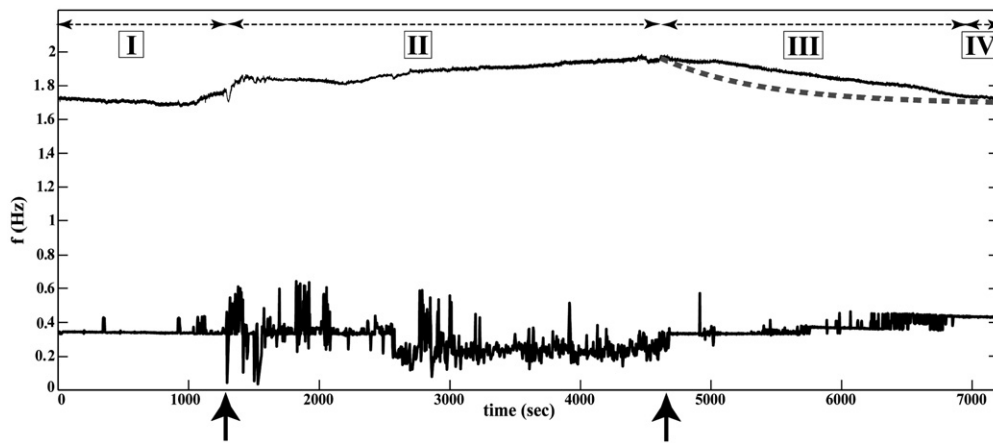


Fig. 2 Heart rate of the patient P05 during the 2 h time interval (before, during and after the SBT) (top, solid line). Markov chain model prediction of the heart rate relaxation in phase III (top, dashed line). Respiration rate of the patient P05 during the same time interval (bottom, solid line). Arrows on the time axis (at the bottom) indicate the beginning and the end of SBT.

We observed a negative correlation (Spearman $\rho_S = -0.625$, $P = .003$) between the total accuracy of the prediction ε_{dm} and the patients sedation level (Fig. 3). All of the patients for whom HRR was successfully predicted were either sleeping long-term tracheostomy patients at least somewhat sedated with one of the two common sedating drugs (propofol, midazolam) (see Table 1). The patients for whom our model failed were incompletely sedated patients with an endotracheal tube traversing the vocal cords.

Table 2 Relaxation time constants of the heart rate relaxation in phase III and MAPE errors^a

Patient	Data set	T_{fit} , s	T_{model} , s	ε_{md} , %	ε_{df} , %	ε_{mf} , %
P01	D01	1703.87	659.51	1.83	1.77	0.81
P02	D02	663.57	627.92	1.03	1.03	0.11
P03	D03	1299.71	1517.12	2.98	1.67	2.04
P04	D04	59.21	51.94	2.19	2.07	0.89
P05	D05	451.06	448.60	2.59	2.41	0.46
P06	D06	127.32	71.69	1.35	1.21	0.75
P07	D07	260.82	342.23	1.05	0.90	0.44
P08	D08	353.48	281.63	1.73	1.64	0.97
	D09	117.33	92.89	2.59	2.81	0.55
	D10	192.60	253.10	3.71	3.43	1.30
P09	D11	5643.34	793.37	4.13	0.44	4.14
P10	D12	41.24	30.88	1.18	1.17	0.24
P11	D13	66.53	53.98	1.69	1.39	1.05
P12	D14	201.21	173.51	0.77	0.58	0.58
	D15	42.63	31.76	2.35	1.90	2.05
P13	D16	689.66	750.89	2.35	2.28	0.86
	D17	1799.21	131.14	3.30	1.60	2.78
P14	D18	231.00	218.73	3.65	2.96	1.60
P15	D19	284.17	6.19	5.21	4.21	2.89
P16	D20	381.97	421.54	1.83	1.67	0.57

^a T_{fit} , exponential fit of observed HR data sets; T_{model} , model prediction, Eq. (10); ε_{md} , L1 distance (MAPE error) between observed HR and predicted HR data sets; ε_{df} , L1 distance (MAPE error) between observed HR data sets and their exponential fits; ε_{mf} , L1 distance (MAPE error) between predicted HR and exponential fit of observed HR data sets.

Interestingly, we also observed a negative correlation (Spearman $\rho_S = -0.446$, $P = .049$) between the ε_{df} error and the sedation level (Fig. 4). This observation indicates that the more patients are sedated the closer is their HRR to an exponential. This explains why our model can better predict HRR of the sedated patients. Indeed, an alternative interpretation of our Markov chain model [Eq. (8)] is that it attempts to predict an optimal exponential fit of the actual heart rate relaxation dynamics.

In fact, because our model can predict only exponential relaxations and since both initial and final values of the heart rate, $f_0 = f(t_0)$ and $\langle f \rangle_{IV}$, are given as the input to our model (they are taken from the data in phases II and IV, respectively), the sole prediction generated is the relaxation time, T_{off} [Eq. (10)]. Thus, another way to estimate the quality of the model predictions is to compare the predicted HRR time constants T_{model} with the corresponding time constants T_{fit} obtained from the exponential fit of the actual

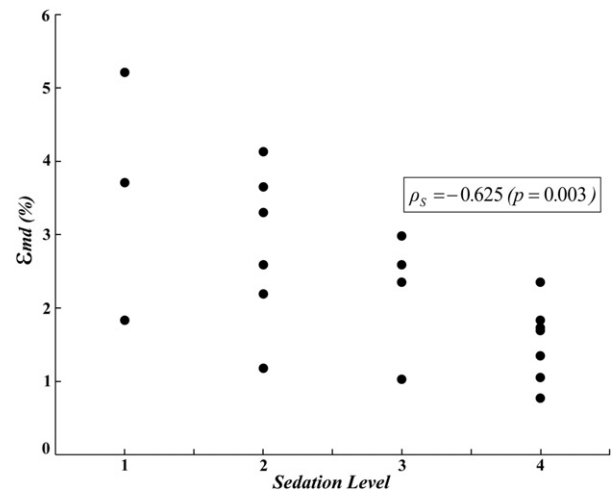


Fig. 3 Scatter plot of the patient's sedation level and the total prediction error, ε_{md} (the distance between predicted and actual HR data sets). Spearman correlation coefficient $\rho_S = -0.625$ ($P = .003$).

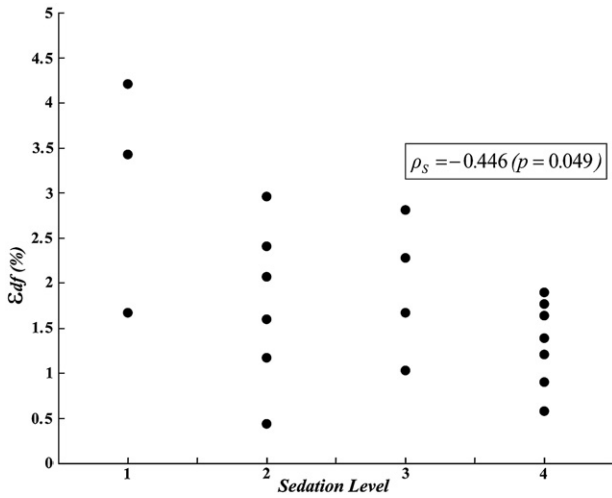


Fig. 4 Scatter plot of the patient’s sedation level and the error of the exponential fit of observed HR data sets, ε_{dff} (the distance between observed HR data sets and their exponential fits). Spearman correlation coefficient $\rho_S = -0.446$ ($P = .049$).

HRR data. The values of T_{model} and T_{fit} for all 20 data sets are presented in Table 2, and scatter plot of T_{model} vs. T_{fit} is shown on Fig. 5. The Fig. 5 clearly shows that most of the points lie along the diagonal of the scatter plot except the three outliers that correspond to the data sets D01, D11, and D17. There is a significant correlation between the predicted and observed time constants (Pearson correlation coefficient $R = 0.484$, $P = .030$); when the 3 outliers are removed, the correlation becomes nearly perfect ($R = 0.975$, $P < 10^{-3}$).

5. Discussion

5.1. Markov chain model and the linear response approximation

We have used Markov Chain theory to derive the relation between poststress HRR time constants and a simple time domain measure of HRV during “steady-state”

stress [Eq. (10)]. This relation was derived under Gaussian, one-step memory assumptions and connects two linear measures of the HR dynamics. These assumptions limit the model.

1. The model postulates a Gaussian probability distribution for the HR. Here, the model produced an exponential decay (HRR)—a typical linear response. The correlation coefficient of the Poincaré plot is also a Gaussian measure of a time series (even if the Poincaré plot itself is a nonlinear representation of the data) and can be expressed in terms of the standard Gaussian time-domain measures of HR time series: variance (SDNN) and covariance (SDSD) [35].
2. The Markov chain model contains a one-step memory approximation. In our case the model further postulates Gaussian probability distributions for the HR, a postulate that makes the analytical calculations possible but is known to be incorrect; HR distributions over very long time intervals (much longer than the SBT) more typically approximate a Lévy flight [39].

This oversimplified Gaussian, one-step memory framework nevertheless produced useful predictions for most—but not all—data sets. The most glaring model failure (where the HRR appeared to be a combination of a power law with almost linear decay instead of the exponential form) is shown in Fig. 2 (patient P09). The curvatures of the actual data and our prediction have opposite signs: the patient’s HRR is a convex function of time, whereas the prediction is always exponential and thus always concave. More generally, the simplifications of the model mean that every HRR dynamic with this convex curvature will defy prediction. Why the HRR displays opposite curvature is unknown. Nevertheless, the nonexponential HRR phenomenon has been observed in other models of cardiac stress, including standard treadmill exercise tests. For example, it was found in Ref. [14] that the first order exponential fit systematically failed to capture the actual character of HRR dynamics in their patients, and thus,

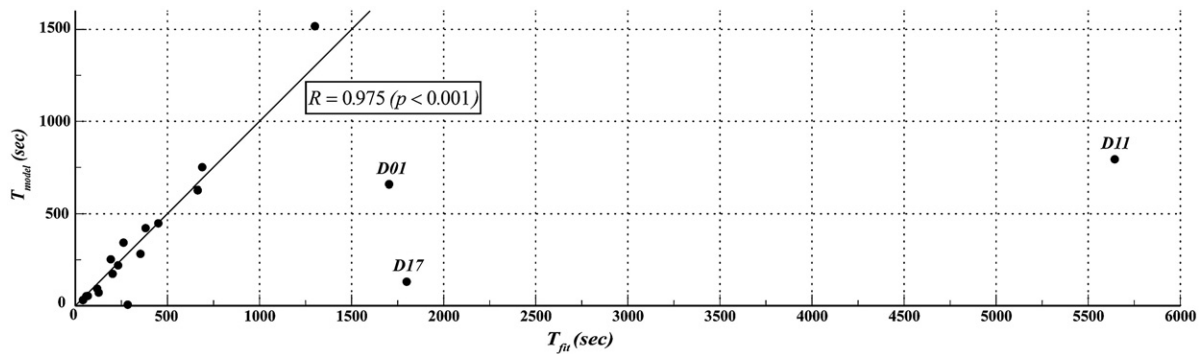


Fig. 5 Scatter plot of the predicted HRR time constants T_{model} [Eq. (10)] vs. time constants T_{fit} obtained from the exponential fit of observed HRR data sets. Most of the data points lie along the diagonal. The outliers correspond to the data sets D01, D11 and D17. Pearson correlation coefficient (without outliers) $R = 0.975$ ($P < .001$).

a second order exponential fit was selected. Where the ANS is disrupted (such as in cardiac transplant patients), HRR appears to be linear [38].

Our finding that the accuracy of the model prediction appears to be negatively correlated with the patient sedation level may in fact be directly related to the use of Markov chain one-step memory approximation. It is understood that normal (healthy) physiological dynamics (including HR dynamics) has long range (time) memory [39]. In contrast, the HR dynamics during a disease or aging loses its “complexity” [40,41] and becomes a shorter range memory process. A Markov Chain approximates a short range (one-step) memory dynamics. Since sedation “disconnects” higher brain regulation from cardiac and respiratory systems, it is possible (see Refs. [42-45]) that the “uncoupled” heart dynamics indeed becomes a process with a short range memory. Thus, strongly sedated patients become more “Markovian”; we speculate this is why our linear response approximations work better for these patients. This speculation is at least consistent with the recent results of Yulmetyev et al [46] who developed a quantitative measure of non-Markovity, applied it to the HRV analysis [47] and demonstrated that the degree of HR Markovity is significantly higher in elderly as compared to young people [48].

Another assumption used in our Markov Chain model is the “weak-sense” stationarity of the HR data (stationarity of mean and standard deviation). It is also possible that the HR dynamics of strongly sedated patients are more stationary, and that is the reason why the model predictions are better for these patients. A systematic study (with larger number of data sets) that would include formal statistical tests of Markovity (such as developed in [46-48]), stationarity, and Gaussian statistics is needed in order to determine the violation of which assumption, namely, long-range memory, strong nonstationarity, or significant non-Gaussian statistics contribute most to the model failure.

Finally, the use of linear response theory assumes that the stress is relatively modest, or that probability distribution is Gaussian. Eq. (8) may not be valid in case of HRR beyond some threshold level of stress or whenever ANS tone modulates HR too strongly. Thus, the exact scope of the validity of Eq. (8) remains to be established.

5.2. Model verification

The HR data we used to test our theoretical predictions have limitations on clinical generalizability. For this pilot study, the data were collected from a convenience cohort. The cohort was small (16 patients) and inhomogeneous with respect to age, sex, ethnicity, and indication for ICU admission. More experimental data are needed to validate theory, perhaps including the HR data from experimental exercise ergometry obtained from both healthy subjects as well as those with acute and chronic diseases affecting the cardiovascular system. Such ambulatory subjects have more

robust physiologies than patients on life support in intensive care units.

As noted, it is not straightforward to compare our theoretical predictions [Eq. (10)] with the available experimental results from (for example) treadmill stress tests because in nearly all previous studies ([49] is an exception), the statistical analysis has been done on the heart period (interbeat or R-R-interval) data, not on HR (instantaneous frequency) itself. Because the relationship between HR and R-R intervals is reciprocal and, thus, inherently nonlinear, any HRV indices (eg, Poincaré plot or power spectra) calculated from R-R intervals could well be different from the same HRV indices calculated from HR (see, eg, Ref. [22] and references therein). Additional analysis of both our model and of data is required in order to verify and extend our theoretical results and also to establish the interval over which Eq. (10) is valid.

5.3. Additional considerations

We note that if stress is sufficiently long, it is possible to compute the probabilities [Eqs. (2-3)] directly from the HR data sets (eg, from 2D histogram $f(n)$ vs. $f(n+1)$), which is yet another representation of the Poincaré plot and thereby avoid assumptions about Gaussian probability distribution, solve the propagation equation Eq. (6) numerically (with an “empirical” transition matrix R) using the approach described in the Section 3.3. Even our present approach completely individualizes the prediction for HRR of any given patient after a given stress. This becomes a physiological instance of “personalized medicine.”

Using the proposed approach, one could extract new information from the data obtained from traditional stress tests or other perturbations. We note that the method is not limited to the analysis of the HR. Rather, it can be applied to analyze the response of other physiological signals (eg, blood pressure or respiration) to many different perturbations (eg, drugs). Other SBT-related responses that can be analyzed with our method include minute ventilatory recovery time (V_{ERT}) after the SBT, which recently was established as a predictor of extubation outcome [50-52].

6. Conclusions

In summary, we developed a Markov chain model of HR dynamics during and after a physiologic stress. We obtained an analytical solution that connects the poststress HRR time constant and an index (correlation coefficient of HR Poincaré plot) of HRV during a steady-state stress. We tested this relationship with the data we recorded during the SBTs in mechanically ventilated critically ill patients. For 17 out of 20 of the SBTs, we were able to correctly predict the post-SBT HRR time constants using HRV during the SBT. The method

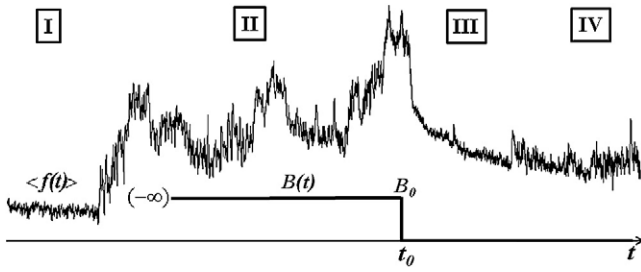


Fig. 6 Heart rate $\langle f(t) \rangle$ of the patient P05 (top) and the schematic representation of the stress (perturbation) function $B(t)$ (bottom) used in derivation of the Eq. (10) from the fluctuation-dissipation theorem (see Appendix A).

used here to predict physiologic dynamics may be applicable to other reversible stresses and other physiologic systems.

Appendix A. Derivation of the relationship between HRR and HRV from the fluctuation-dissipation theorem

In this appendix, the relation between poststress recovery of heart rate (heart rate recovery, HRR) (phase III) and HRV during the stress (phase II) is derived using the fluctuation-dissipation theorem.¹⁰

We consider a stress (phase II) as a constant perturbation of the HR dynamics $f(t)$ that has been “on” for a rather long (“infinite”) time (so the HR has reached a steady-state during the stress) and is then switched off at time t_0 (end of the stress, see Fig. 6). Then the HR relaxes (phase III) to the new steady-state (which is HR at rest, phase IV). Thus we assume that HR in both phase II and in phase IV are at steady state.

We can describe the termination of the stress as a step-off function:

$$B(t) = B_0 \theta[-(t - t_0)] = B_0 \theta(t_0 - t) \quad (\text{A1})$$

where θ is a Heaviside function and $B_0 = \text{const}$ is the stress intensity.

Provided that the perturbation (stress intensity) B_0 is small, one can apply the fluctuation-dissipation theorem and express the relaxation from the stress (HRR) (phase III) as [25,53]:

$$\langle f(t_k) \rangle_{III} = \langle f \rangle_{IV} + \frac{B_0}{kT} \cdot \langle \delta f(t) \delta f(t + t_k) \rangle_{II} \quad (\text{A2})$$

where $\langle f \rangle_{IV} = \text{const}$ is average HR in the phase IV (at steady-state), $C(t_k) = \langle \delta f(t) \delta f(t + t_k) \rangle_{II}$ is the autocorrelation (autocovariance) function during phase II (also steady-state), and $t_k = t_0 + k \Delta t$.

¹⁰ This approach rests on the assumption that there is an underlying, effective, time-independent Hamiltonian for the HRV, which predicts steady-state behavior at long-times. This assumption is less restrictive than the Gaussian, Markov assumption of the main text. For a non-Gaussian process, the predictions of the fluctuation-dissipation theorem, however, are limited to small perturbations.

By analogy to the temperature of a fluctuating physical particle, the “thermal energy” of HR fluctuations (HRV) can be written as:

$$kT \sim \sigma_f^2 = \langle \delta f^2 \rangle \quad (\text{A3})$$

(the “width” of the HR distribution, $\sigma_f \sim \sqrt{kT}$). We can define the stress intensity as

$$B_0 \approx \Delta f = \langle f \rangle_{II} - \langle f \rangle_{IV}, \quad (\text{A4a})$$

where $\langle f \rangle_{II}$ and $\langle f \rangle_{IV}$ are average (expectation value) HRs in phase II and in phase IV respectively. This is actually the simplest definition of the stress intensity, namely the difference between the current HR and the baseline (HR at rest). Because the HR in phase II is at steady-state, the average $\langle f \rangle_{II}$ does not depend on time, so $\langle f \rangle_{II} \approx \langle f(t_0) \rangle_{II} \approx f_0$ and

$$B_0 \approx \Delta f = f_0 - \langle f \rangle_{IV} \quad (\text{A4b})$$

Note that these “intuitive” definitions of the stress level B_0 (A4) and the thermal energy kT (A3), are consistent and, in fact, are not independent: at the time moment $t_k = t_0$ (beginning of HRR), the autocorrelation function is $C(t_0) = \langle \delta f^2 \rangle \equiv \sigma_f^2$ and the Eq. (A2) becomes:

$$f_0 = \langle f \rangle_{IV} + \frac{B_0}{kT} \cdot \sigma_f^2 \quad (\text{A5})$$

So if we postulate one of the definitions [Eq. (A3) or Eqs. (A4a, A4b)] the other one can be obtained from the Eq. (A5) (initial conditions). Thus, Eq. (A2) becomes:

$$\langle f(t_k) \rangle_{III} = \langle f \rangle_{IV} + (f_0 - \langle f \rangle_{IV}) \frac{\langle \delta f(t) \delta f(t + t_k) \rangle_{II}}{\langle \delta f^2 \rangle_{II}} \quad (\text{A6})$$

The challenge of calculation of the HRR is thereby transformed into the simpler challenge of calculation of the HR autocorrelation function. The challenge is “simpler” because autocorrelation functions are known for common processes.

The exponentially decaying autocovariance function (used in the main text of the article) can be written as (see, eg, Ref. [36]) $C(k) = \langle \delta f(n) \delta f(n+k) \rangle_{II} = \sigma_f^2 r^k$. Note that $C(0) = \sigma_f^2 \equiv \langle \delta f^2 \rangle_{II}$ and so $r = \frac{C(1)}{C(0)} = \frac{\langle \delta f(n) \delta f(n+1) \rangle_{II}}{\langle \delta f^2 \rangle_{II}}$ or, in terms of time steps: $r_{ff}(\Delta t) = \frac{\langle \delta f(t) \delta f(t + \Delta t) \rangle}{\langle \delta f^2 \rangle} \equiv \frac{\langle \delta f(t - \Delta t) \delta f(t) \rangle}{\langle \delta f^2 \rangle}$. This leads to a discrete expression:

$$\langle f(k) \rangle_{III} = \langle f \rangle_{IV} + (f_0 - \langle f \rangle_{IV}) \cdot r^k \quad (\text{A7})$$

or, in terms of time steps,

$$\langle f(t_k) \rangle_{III} = \langle f \rangle_{IV} + (f_0 - \langle f \rangle_{IV}) \cdot [r_{ff}(\Delta t)]^{\frac{t_k - t_0}{\Delta t}} \quad (\text{A8})$$

Or, equivalently,

$$\langle f(t_k) \rangle_{III} = \langle f \rangle_{IV} + (f_0 - \langle f \rangle_{IV}) \cdot \exp[-(t_k - t_0)/T_{off}] \quad (\text{A9})$$

where

$$T_{off} = \frac{\Delta t}{|\ln[r_{ff}(\Delta t)]|} \quad (\text{A10})$$

Appendix B. On the relationships among Poincaré plots, Markov Chains and first-order autoregressive processes

In this appendix we provide a concise summary of the main mathematical concepts used in the paper and emphasize the connections between them.

A Poincaré plot (a standard method of the HRV analysis) is usually defined as a set of points (RR_k, RR_{k+1}) so each point corresponds to two consecutive R-R intervals. More specifically, the original sequence of R-R intervals $(RR_1, RR_2, \dots, RR_{K-1}, RR_K)$ is used to construct two sequences, $RR_x = (RR_1, RR_2, \dots, RR_{K-1})$ and $RR_y = (RR_2, RR_3, \dots, RR_K)$. The plot of RR_x vs RR_y is then called a ‘‘Poincaré plot.’’ The version of the Poincaré plot we used in the paper has two modifications. First, instead of plotting R-R intervals, we plot HR intervals which are the inverse values: $HR_k = 1/RR_k$. Second, instead of using the ‘‘raw’’ sequence of HR, we interpolate them at the constant sampling rate, $(\Delta t)^{-1}$. For clarity, we use the notation $f_k \equiv f(t_k)$ (instead of HR_k) for the interpolated HR. We choose the sampling rate to be equal to the mean HR, so $\Delta t = \langle f \rangle^{-1}$. The Poincaré plot of $f(t_k)$ vs $f(t_{k+1}) \equiv f(t_k + \Delta t)$ is shown in Fig. 7 (center).

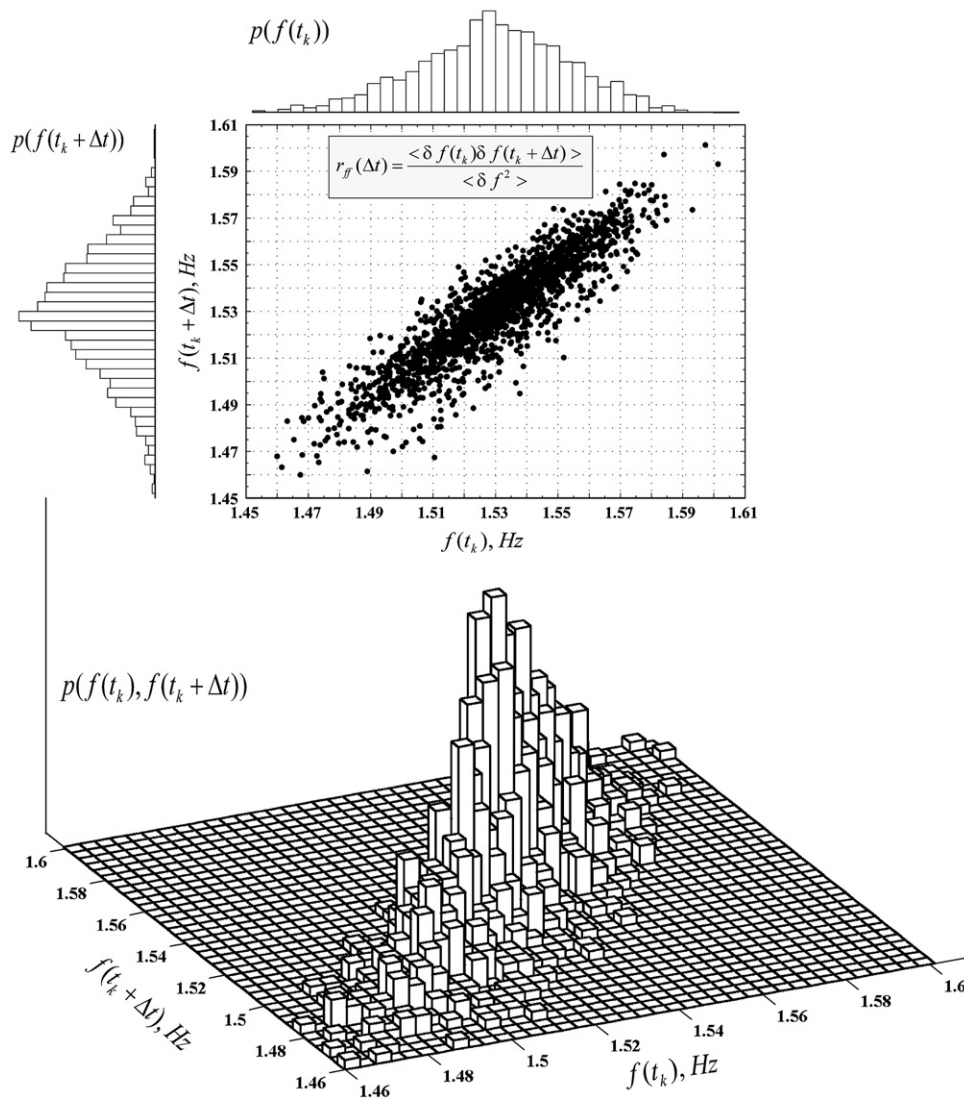


Fig. 7 On the relationship between the Poincaré plot and Markov Chain model (see Appendix B for details). Poincaré plot of the consecutive interpolated HR intervals (patient P05) {inset: definition of the Pearson correlation coefficient of the Poincaré plot [Eq. (9)]} (center). Projections of the data points to the axes of the Poincaré plot: HR probability distributions [Eq. (2)] (top and left). Representation of the Poincaré plot as a 3D histogram (bottom). The vertical axis defines the ‘‘one-step’’ joint probability distribution [Eq. (3)].

Pearson correlation coefficient of the Poincaré plot is defined as the correlation coefficient between RR_x and RR_y data sets (“one step correlation”). In our notation, the correlation coefficient is [compare to the Eq. (9) in the article]:

$$r_{ff} \equiv \frac{\text{cov}(f_k, f_{k+1})}{\sigma_{f_k} \sigma_{f_{k+1}}} = \frac{\langle (f(t_k) - \langle f \rangle)(f(t_k + \Delta t) - \langle f \rangle) \rangle}{\sigma_f^2} = \frac{\langle \delta f(t_k) \cdot \delta f(t_k + \Delta t) \rangle}{\langle \delta f^2 \rangle} \quad (\text{B1})$$

Projections of the data cloud on the x and y axes (the histograms on the top and left of the Poincaré plot on the Fig. 7) define the probability distributions of, respectively, $f(t_k)$ and $f(t_k + \Delta t)$. These probability distributions $\{p[f(t_k)]$ and $p[f(t_k + \Delta t)]\}$ were used in our Markov Chain model [Eq. (2)] where they were assumed to be identical and have Gaussian shapes (normal distributions). Note that the same assumptions are used in the HRV analysis, where the RR_k , and RR_{k+1} histograms are assumed to be identical and are characterized only by their mean and standard deviation (which is essentially the assumption of their normality).

It is possible to visualize the Poincaré plot as 3D histogram [see Fig. 7 (bottom)]. In such a representation, the height of the histogram bar represent the relative number of times that a pair of consecutive R-R (or HR) values were found in the data set (see, eg, Ref. [54]). Thus, the 3D representation of the Poincaré plot defines the joint probability distribution $p[f(t_k), f(t_k + \Delta t)]$ used in the Markov Chain model [Eq. (3) in the article]. In our model, this probability was assumed to be a 2D Gaussian, which roughly corresponds to the shape of the actual data (see the Fig. 7) and also is a consequence of our previous assumption about the normality of the individual probability distributions $p[f(t_k)]$ and $p[f(t_k + \Delta t)]$.

If the HR data set is sufficiently long, both single and joint probability distributions can be calculated directly from the data (using the Poincaré plot) without the assumptions about the normality of these distributions. Thus, the Poincaré plot (in its 3D form) of a dynamical system contains all the information needed to construct both single and joint probability distributions and thus to build Markov Chain model of that dynamical system.

Note that the Eq. (3) for the joint probability distribution $p[f(t_k), f(t_k + \Delta t)]$ is an instance of the joint probability distribution $p(x, y)$ of 2 Gaussian random variables, x and y :

$$p(x, y) = \frac{1}{2\pi\sigma_x\sigma_y\sqrt{1-r^2}} \exp \left\{ -\frac{1}{2(1-r^2)} \left[\frac{(x-\langle x \rangle)^2}{\sigma_x^2} - \frac{2r(x-\langle x \rangle)(y-\langle y \rangle)}{\sigma_x\sigma_y} + \frac{(y-\langle y \rangle)^2}{\sigma_y^2} \right] \right\} \quad (\text{B2})$$

where $r = \frac{\text{cov}(x, y)}{\sigma_x\sigma_y}$ is the coefficient of correlation between x and y . If we put $x = f(t_k)$ and $y = f(t_{k+1}) \equiv f(t_k + \Delta t)$ (so that $\langle x \rangle = \langle y \rangle = \langle f \rangle$ and $\sigma_x = \sigma_y = \sigma_f$), we obtain Eq. (3) of the main paper for one-step joint probability. The Eq. (B3) [in the form of Eq. (3)] is used to fit the ellipse to the HR Poincaré plot (in order to calculate the main axes SD1 and SD2 see [35] for the discussion).

Finally, we show the connection of the correlation coefficient of the Poincaré plot to the 1st order autoregressive process AR(1). Assume that the heart rate dynamics can modeled by AR(1), that is:

$$\delta f(t_{k+1}) = r \cdot \delta f(t_k) + \xi(t_k) \quad (\text{B3})$$

Here r is the AR(1) parameter, ξ is a noise term [36], $t_k = k\Delta t$, and Δt is a step size. The autocovariance function of the AR(1) process can be written as [36]:

$$C(t_k) = \langle \delta f(t) \delta f(t + t_k) \rangle_t = \sigma_f^2 \cdot r^{\frac{t_k}{\Delta t}} \equiv \sigma_f^2 \cdot \exp(-t_k/T_{\text{off}}) \quad (\text{B4})$$

where

$$T_{\text{off}} = \frac{\Delta t}{|\ln r|} \quad (\text{B5})$$

Note that $C(t_0) = \sigma_f^2 \equiv \langle \delta f^2 \rangle_{\text{II}}$ and thus $r = \frac{C(t_1)}{C(t_0)} = \frac{\langle \delta f(t) \delta f(t + \Delta t) \rangle}{\langle \delta f^2 \rangle} \equiv r_{ff}(\Delta t)$. So the correlation coefficient of the Poincaré plot [$f(t_k)$ vs. $f(t_{k+1})$] can be viewed as a parameter of the corresponding AR(1) process and also defines the relaxation time of the autocovariance (autocorrelation) function of that process [compare Eq. (B5) to the Eq. (10) in the article]. In this case T_{off} also characterizes relaxations of “microscopic” fluctuations (HRV) of the HR dynamics at rest¹¹.

Since AR(1) is a Markov Process, both AR(1) and Markov Chains have the same “one-step memory”: the value at the next step $f(t_{k+1})$ depends only on the value at the current step $f(t_k)$ but not on the previous steps. This also is the reason why they both are related to the Poincaré plot, which is used to visualize the correlation between *consecutive* R-R (or HR) intervals (“one-step correlation”).

¹¹ This result reflects the famous Onsager “regression hypothesis” [25] (the physical basis of the fluctuation dissipation theorem): the same T_{off} characterizes both the decay of spontaneous “microscopic” fluctuations (HRV) of the HR at rest and “macroscopic” relaxation (HRR) of the HR to a new steady-state after a relatively small perturbation.

The approaches described above can be applied to the analysis of HR resampled at different frequencies $(\Delta t)^{-1}$ and a sequence of the Poincaré plots and the corresponding relaxation times T_{off} can be constructed. Note that this approach is different from the so-called “lagged” Poincaré plot method [35] where the values $[f(t_k) \text{ vs } f(t_{k+m})]$ are plotted. In our case the Poincaré plot is always “the first return map” $[f(t_k) \text{ vs } f(t_{k+1}) \equiv f(t_k + \Delta t)]$, but the sampling time interval Δt varies (so Poincaré plots at different sampling times have different number of points). It is also somewhat different from the widely used “coarse-graining” approach [37] because we use interpolation instead of coarse-graining. It remains to be seen whether any new useful information regarding HRR or HRV in general can be obtained using such a multiscale analysis (see Ref. [55] for the application of this approach to the analysis of the dynamics of an abstract mathematical model).

Appendix C. Derivation of Eq. (8)

We have used the following notations (see the main text):

$$\mathbf{R} = \mathbf{R}' \cdot df; f_i = (S_i - 0.5 \cdot L); \delta f_i = f_i - \langle f \rangle; \chi(0) = \langle \delta f(t)^2 \rangle; \chi(1) = \langle \delta f(t - \Delta t) \delta f(t) \rangle$$

The Eq. (7) reads:

$$\langle f(t_k) \rangle = \sum_{n=1}^N f_n \cdot P_n(t_k) = \sum_{j=1}^N \sum_{i=1}^N f_i \cdot [R^k]_{ij} \cdot P_j(t_0), \text{ where } t_k = t_0 + k\Delta t; \mathbf{P}(t_k) = \mathbf{R}^k \cdot \mathbf{P}(t_0)$$

Suppose $f(t_0) = f_j$, then $P_n(t_0)$ is defined as follows: $P_n(t_0) = 1$ for $n = j$ and 0 elsewhere. $n, j = 1, \dots, N$.

First we calculate one-step sum $\sum_{i=1}^N f_i \cdot [R^k]_{ij} (k=1)$:

$$\begin{aligned} \sum_{i=1}^N f_i \cdot R(f_i|f_j) &= \int_{f_i}^{f_N} (\delta f_i + \langle f \rangle) \cdot R'(f_i|f_j) d(f_i) \\ &\cong \int_{-\infty}^{\infty} (\delta f_i + \langle f \rangle) \cdot R'(f_i|f_j) d(\delta f_i) \\ &= \langle f \rangle + \int_{-\infty}^{\infty} (\delta f_i \cdot R'(f_i|f_j)) d(\delta f_i) \\ &= \langle f \rangle + \int_{-\infty}^{\infty} (\delta f_i \cdot \sqrt{\frac{\chi(0)}{2\pi|M|}} \exp\left\{-\frac{1}{2[\chi^2(0) - \chi^2(1)]} [\chi(0)(\delta^2 f_j + \delta^2 f_i) - 2\chi(1)\delta f_j \delta f_i] + \frac{1}{2} \frac{\delta^2 f_j}{\chi(0)}\right\} d(\delta f_i) \\ &= \langle f \rangle + \sqrt{\frac{\chi(0)}{2\pi|M|}} \int_{-\infty}^{\infty} y \cdot \exp\left\{-\frac{\chi(0)}{2[\chi^2(0) - \chi^2(1)]} \left[y - \frac{\chi(1)}{\chi(0)} \cdot \delta f_j\right]^2\right\} dy \\ &= \langle f \rangle + \sqrt{\frac{\chi(0)}{2\pi|M|}} \int_{-\infty}^{\infty} \left(y - \frac{\chi(1)}{\chi(0)} \cdot \delta f_j\right) \cdot \exp\left\{-\frac{\chi(0)}{2[\chi^2(0) - \chi^2(1)]} \left[y - \frac{\chi(1)}{\chi(0)} \cdot \delta f_j\right]^2\right\} dy \\ &\quad + \frac{\chi(1)}{\chi(0)} \cdot \delta f_j \cdot \sqrt{\frac{\chi(0)}{2\pi|M|}} \int_{-\infty}^{\infty} \exp\left\{-\frac{\chi(0)}{2[\chi^2(0) - \chi^2(1)]} \left[y - \frac{\chi(1)}{\chi(0)} \cdot \delta f_j\right]^2\right\} dy \end{aligned}$$

Denote $z = y - \frac{\chi(1)}{\chi(0)} \cdot \delta f_j$

$$\begin{aligned} I &= \langle f \rangle + \sqrt{\frac{\chi(0)}{2\pi|M|}} \int_{-\infty}^{\infty} z \cdot \exp\left\{-\frac{\chi(0)}{2[\chi^2(0) - \chi^2(1)]} \cdot z^2\right\} dz \\ &\quad + \frac{\chi(1)}{\chi(0)} \cdot \delta f_j \cdot \sqrt{\frac{\chi(0)}{2\pi|M|}} \int_{-\infty}^{\infty} \exp\left\{-\frac{\chi(0)}{2[\chi^2(0) - \chi^2(1)]} \cdot z^2\right\} dz \end{aligned}$$

Using the following identities

$$\sqrt{\frac{\chi(0)}{2\pi|M|}} \int_{-\infty}^{\infty} \exp\left\{-\frac{\chi(0)}{2[\chi^2(0) - \chi^2(1)]} \cdot z^2\right\} dz = 1; \int_{-\infty}^{\infty} z \cdot \exp\left\{-\frac{\chi(0)}{2[\chi^2(0) - \chi^2(1)]} \cdot z^2\right\} dz = 0$$

We obtain $I = \langle f \rangle + \frac{\chi(1)}{\chi(0)} \cdot \delta f_j$
 At the arbitrary step k , we get: $\sum_{i=1}^N f_i \cdot R^k(f_i|f_j) = \langle f \rangle + \left[\frac{\chi(1)}{\chi(0)} \right]^k \cdot \delta f_j$
 Finally, using Eq. (7), we obtain:

$$\begin{aligned} \langle f(t_k) \rangle &= \sum_{j=1}^N \sum_{i=1}^N f_i \cdot [R^k]_{ij} \cdot P_j(t_0) \\ &= \sum_{j=1}^N \left\{ \left[\frac{\chi(1)}{\chi(0)} \right]^k \cdot \delta f_j + \langle f \rangle \right\} \cdot P_j(t_0) \left(\sum_{j=1}^N \delta f_j \cdot P_j(t_0) = \sum_{j=1}^N (f_j - \langle f \rangle) \cdot P_j(t_0) = f(t_0) - \langle f \rangle \right) \\ &= \langle f \rangle + \left[\frac{\chi(1)}{\chi(0)} \right]^k \cdot (f(t_0) - \langle f \rangle) \\ &= \langle f \rangle + (f(t_0) - \langle f \rangle) \cdot \exp \left[-\frac{t_k - t_0}{\Delta t} \ln \frac{\chi(0)}{\chi(1)} \right] \end{aligned}$$

References

- [1] Shephard R. Exercise physiology. Philadelphia: BC Decker Inc.; 1987.
- [2] Pierpont GL, Voth EJ. Heart rate recovery from exercise as an index of both parasympathetic and sympathetic activity. *FASEB J* 2002;16(5): A1142.
- [3] Imai K, Sato H, Hori M, Kusuoka H, Ozaki H, Yokoyama H, et al. Vagally mediated heart rate recovery after exercise is accelerated in athletes but blunted in patients with chronic heart failure. *J Am Coll Cardiol* 1994;24(6):1529-35.
- [4] Buchheit M, Papelier Y, Laursen PB, Ahmadi S. Noninvasive assessment of cardiac parasympathetic function: postexercise heart rate recovery or heart rate variability? *Am J Physiol Heart Circ Physiol* 2007;293(1):H8-H10.
- [5] Kannankeril PJ, Goldberger JJ. Parasympathetic effects on cardiac electrophysiology during exercise and recovery. *Am J Physiol Heart Circ Physiol* 2002;282(6):H2091-8.
- [6] Goldberger JJ, Le FK, Lahiri M, Kannankeril PJ, Ng J, Kadish AH. Assessment of parasympathetic reactivation after exercise. *Am J Physiol Heart Circ Physiol* 2006;290(6):H2446-52.
- [7] Lauer M, Froelicher ES, Williams M, Kligfield P. Exercise testing in asymptomatic adults: a statement for professionals from the American Heart Association Council on Clinical Cardiology, Subcommittee on Exercise, Cardiac Rehabilitation, and Prevention. *Circulation* 2005;112(5):771-6.
- [8] Shetler K, Marcus R, Froelicher VF, Vora S, Kalisetti D, Prakash M, et al. Heart rate recovery: validation and methodologic issues. *J Am Coll Cardiol*, 2001;38(7):1980-7.
- [9] Morise AP. Heart rate recovery: predictor of risk today and target of therapy tomorrow? *Circulation* 2004;110(18):2778-80.
- [10] Smith LL, Kukielka M, Billman GE. Heart rate recovery after exercise: a predictor of ventricular fibrillation susceptibility after myocardial infarction. *Am J Physiol Heart Circ Physiol* 2005;288(4): H1763-9.
- [11] Seshadri N, Gildea TR, McCarthy K, Pothier C, Kavuru MS, Lauer MS. Association of an abnormal exercise heart rate recovery with pulmonary function abnormalities. *Chest* 2004;125(4):1286-91.
- [12] Cole CR, Foody JM, Blackstone EH, Lauer MS. Heart rate recovery after submaximal exercise testing as a predictor of mortality in a cardiovascularly healthy cohort. *Ann Intern Med* 2000;132(7):552-5.
- [13] Nishime EO, Cole CR, Blackstone EH, Pashkow FJ, Lauer MS. Heart rate recovery and treadmill exercise score as predictors of mortality in patients referred for exercise ECG. *JAMA* 2000;284(11):1392-8.
- [14] Gorelik DD, Hadley D, Myers J, Froelicher V. Is there a better way to predict death using heart rate recovery? *Clin Cardiol* 2006;29(9):399-404.
- [15] Javorka M, Zila I, Balharek T, Javorka K. On- and off-responses of heart rate to exercise - relations to heart rate variability. *Clin Physiol Funct Imaging* 2003;23(1):1-8.
- [16] Billman GE. Heart rate response to onset of exercise: evidence for enhanced cardiac sympathetic activity in animals susceptible to ventricular fibrillation. *Am J Physiol Heart Circ Physiol* 2006;291(1):H429-35.
- [17] Ricardo DR, de Almeida MB, Franklin BA, Araujo CGS. Initial and final exercise heart rate transients: influence of gender, aerobic fitness, and clinical status. *Chest* 2005;127(1):318-27.
- [18] Leeper NJ, Dewey FE, Ashley EA, Sandri M, Tan SY, Hadley D, et al. Prognostic value of heart rate increase at onset of exercise testing. *Circulation* 2007;115(4):468-74.
- [19] Javorka M, Zila I, Balharek T, Javorka K. Heart rate recovery after exercise: relations to heart rate variability and complexity. *Braz J Med Biol Res* 2002;35(8):991-1000.
- [20] Camm AJ, Malik M, Bigger JT, Breithardt G, Cerutti S, Cohen RJ, et al. Heart rate variability—standards of measurement, physiological interpretation, and clinical use. *Circulation* 1996;93(5):1043-65.
- [21] Castiglioni P. Evaluation of heart rhythm variability by heart rate or heart period: differences, pitfalls and help from logarithms. *Med Biol Eng Comput* 1995;33(3):323-30.
- [22] Niklasson U, Wiklund U, Bjerle P, Olofsson BO. Heart-rate variation: what are we measuring? *Clin Physiol* 1993;13(1):71-9.
- [23] Pierpont GL, Voth EJ. Assessing autonomic function by analysis of heart rate recovery from exercise in healthy subjects. *Am J Cardiol* 2004;94(1):64-8.
- [24] Kubo R. The fluctuation-dissipation theorem. *Rep Prog Phys* 1966;29(1):255-84.
- [25] Chandler D. Introduction to modern statistical mechanics. New York: Oxford University Press; 1987. [xiii, 274 p].
- [26] Norris JR. Markov chains. Cambridge, UK: Cambridge University Press; 1998.
- [27] Pinsky MR. Breathing as exercise: the cardiovascular response to weaning from mechanical ventilation. *Intensive Care Med* 2000;26(9):1164-6.
- [28] Shen H-N, Lin L-Y, Chen K-Y, Kuo P-H, Yu C-J, Wu H-D, et al. Changes of heart rate variability during ventilator weaning. *Chest* 2003;123(4):1222-8.
- [29] Robertson TE, Mann HJ, Hyzy R, Rogers A, Douglas I, Waxman AB, et al. Multicenter implementation of a consensus-developed, evidence-based, spontaneous breathing trial protocol. *Crit Care Med* 2008;36(10):2753-62.
- [30] Burykin A, Buchman TG. Cardiorespiratory dynamics during transitions between mechanical and spontaneous ventilation in intensive care. *Complexity* 2008;13(6):40-59.
- [31] Niskanen JP, Tarvainen MP, Ranta-Aho PO, Karjalainen PA. Software for advanced HRV analysis. *Comput Methods Programs Biomed* 2004;76(1):73-81.
- [32] Hanggi P, Thomas H. Stochastic processes: time evolution, symmetries and linear response. *Phys Rep* 1982;88(4):207-319.
- [33] Otzenberger H, Gronfier C, Simon C, Charlux A, Ehrhart J, Piquard F, et al. Dynamic heart rate variability: a tool for exploring

- sympathovagal balance continuously during sleep in men. *Am J Physiol Heart Circ Physiol* 1998;44(3):H946-50.
- [34] Kamen PW, Tonkin AM. Application of the Poincare plot to heart-rate-variability—a new measure of functional status in heart-failure. *Aust N Z J Med* 1995;25(1):18-26.
- [35] Brennan M, Palaniswami M, Kamen P. Do existing measures of Poincare plot geometry reflect nonlinear features of heart rate variability? *IEEE Trans Biomed Eng* 2001;48(11):1342-7.
- [36] Kirchgässner G, Wolters J. Introduction to modern time series analysis. Berlin: Springer; 2007 [ix, 274 p].
- [37] Costa MD, Peng CK, Goldberger AL. Multiscale analysis of heart rate dynamics: entropy and time irreversibility measures. *Cardiovasc Eng* 2008.
- [38] Savin WM, Haskell WL, Schroeder JS, Stinson EB. Cardiorespiratory responses of cardiac transplant patients to graded, symptom-limited exercise. *Circulation* 1980;62(1):55-60.
- [39] West BJ, Deering W. Fractal physiology for physicists—levy statistics. *Phys Rep* 1994;246(1-2):2-100.
- [40] Lipsitz LA, Goldberger AL. Loss of complexity and aging—potential applications of fractals and chaos theory to senescence. *JAMA* 1992;267(13):1806-9.
- [41] Kaplan DT, Furman MI, Pincus SM, Ryan SM, Lipsitz LA, Goldberger AL. Aging and the complexity of cardiovascular dynamics. *Biophys J* 1991;59(4):945-9.
- [42] Pincus SM. Greater signal regularity may indicate increased system isolation. *Math Biosci* 1994;122(2):161-81.
- [43] Godin PJ, Buchman TG. Uncoupling of biological oscillators: a complementary hypothesis concerning the pathogenesis of multiple organ dysfunction syndrome. *Crit Care Med* 1996;24(7):1107-16.
- [44] Godin PJ, Fleisher LA, Eidsath A, Vandivier RW, Preas HL, Banks SM, et al. Experimental human endotoxemia increases cardiac regularity: results from a prospective, randomized, crossover trial. *Crit Care Med* 1996;24(7):1117-24.
- [45] Clifford JO, Buchman TG. Sedation modulates recognition of novel stimuli and adaptation to regular stimuli in critically ill adults. *Crit Care Med* 2002;30(3):609-16.
- [46] Yulmetyev R, Hanggi P, Gafarov F. Stochastic dynamics of time correlation in complex systems with discrete time. *Phys Rev E* 2000;62(5):6178-94.
- [47] Yulmetyev R, Hanggi P, Gafarov F. Quantification of heart rate variability by discrete nonstationary non-Markov stochastic processes. *Phys Review E* 2002;65(4):046107-15.
- [48] Yulmetyev RM, Demin SA, Panischev OY, Hanggi P. Age-related alterations of relaxation processes and non-Markov effects in stochastic dynamics of R-R intervals variability from human ECGs. *Physica A* 2005;353:336-52.
- [49] Arai Y, Saul JP, Albrecht P, Hartley LH, Lilly LS, Cohen RJ, et al. Modulation of cardiac autonomic activity during and immediately after exercise. *Am J Physiol Heart Circ Physiol* 1989;256(1):H132-41.
- [50] Martinez A, Seymour C, Nam M. Minute ventilation recovery time: a predictor of extubation outcome. *Chest* 2003;123(4):1214-21.
- [51] Seymour CW, Christie JD, Fuchs BD. Minute ventilation recovery time measured using a new, more practical methodology predicts extubation outcome. *Crit Care Med* 2005;33(12):A113.
- [52] Seymour CW, Halpern S, Christie JD, Gallop R, Fuchs BD. Minute ventilation recovery time measured using a new, simplified methodology predicts extubation outcome. *J Intensive Care Med* 2008;23(1):52-60.
- [53] Kampen NGV. Stochastic processes in physics and chemistry. Rev. and enl. ed. North-Holland: North-Holland personal library; 1992 [xiv, 465 p].
- [54] Marciano F, Migaux ML, Acanfora D, Furgi G, Rengo F. Quantification of Poincare maps for the evaluation of heart rate variability. *Computers in Cardiology 1994 Proceedings. Computers in Cardiology, Inc; 1994. p. 577-80.*
- [55] Thuraisingham RA. Enhancing Poincare plot information via sampling rates. *Appl Math Comput* 2007;186(2):1374-8.